

\mathbb{Z}_2 -vortex lattice in the ground state of the triangular Kitaev-Heisenberg model

Ioannis Rousochatzakis,¹ Ulrich K. Rössler,¹ Jeroen van den Brink,¹ and Maria Daghofer¹

¹IFW Dresden, P.O. Box 27 01 16, D-01171 Dresden, Germany

(Dated: September 27, 2012)

Investigating the classical Kitaev-Heisenberg Hamiltonian on a triangular lattice, we establish the presence of an incommensurate non-coplanar magnetic phase, which is identified as a lattice of \mathbb{Z}_2 vortices. The vortices, topological point defects in the $\text{SO}(3)$ order parameter of the nearby Heisenberg antiferromagnet, are not thermally excited but due to the spin-orbit coupling and arise at temperature $T \rightarrow 0$. This \mathbb{Z}_2 -vortex lattice is stable in a parameter regime relevant to iridates. We show that in the other, strongly anisotropic, limit a robust nematic phase emerges.

PACS numbers: 75.10.Hk, 75.70.Tj, 75.30.Kz

Mott insulators with orbital degrees of freedom [1] have long been a topic in condensed-matter research, because the physics of various transition-metal oxides is governed by anisotropies inherent in electronic orbitals. Apart from the drive to understand these materials, the lowered symmetry can lead to new physical phases, e.g., (spin-) orbital liquids [2–5], topological Mott insulators [6], or fractional Chern insulators [7]. Orbital anisotropies have additionally attracted interest as a highly desirable feature in potential realizations of protected qubits [8, 9].

Iridates have been pointed out as a possible realization of strongly direction-dependent orbital Hamiltonians [10], because their $5d$ electrons feel both substantial correlations and strong spin-orbit coupling. The spin-orbit coupling makes the total angular momentum the relevant quantum number to describe the low-energy states with a single hole in the $5d-t_{2g}$ levels [10–12]. The $j = 1/2$ of the low-energy states takes the role of a spin (and will be referred to as such from now on), but the orbital component heavily influences couplings between ‘spins’ [10, 13]. While interactions in the Mott-insulating square planes of Sr_2IrO_4 are isotropic, they are highly anisotropic in more itinerant compounds [14] and for 90° bond angles [10]. On the honeycomb lattice of Na_2IrO_3 , for example, Ising terms couple a different spin component S^x , S^y , or S^z along the three equivalent lattice directions, as in the famous ‘Kitaev’ model [2, 15] with its anyonic excitations.

In this Letter, we show that such a ‘Kitaev’-type anisotropy on the triangular lattice, a geometry very close to the honeycomb case Na_2IrO_3 , induces an incommensurate (IC) and non-coplanar spin pattern that turns out to be a lattice of \mathbb{Z}_2 vortices. The vortices are topologically stable point defects of $\text{SO}(3)$ order parameters [17], as have long been known to be thermally induced in frustrated Heisenberg antiferromagnets [17–21] as well as in the superfluid A-phase of ^3He [22, 23], and more recently in spinor Bose-Einstein condensates [24]. In contrast to \mathbb{Z} vortices driving Berezinsky-Kosterlitz-Thouless transitions, clockwise and counter-clockwise rotation of a \mathbb{Z}_2 vortex are not topologically distinct, and two \mathbb{Z}_2 vortices can thus annihilate each other.

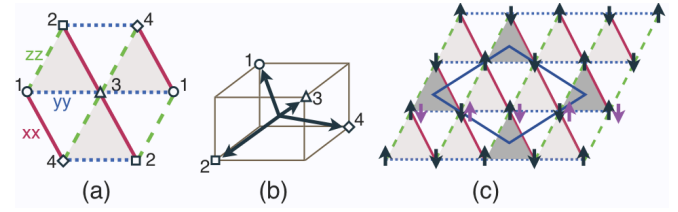


FIG. 1. (color online) (a) Triangular lattice with three types of bonds, “xx”, “yy” and “zz”, see Eq. (1). Sites 1-4 specify the four sublattices for the spin rotations $\mathbf{S} \leftrightarrow \tilde{\mathbf{S}}$ [13]. $\tilde{\mathbf{S}}$ is defined as $\mathbf{S}_1 = \tilde{\mathbf{S}}_1$, $\mathbf{S}_2 = (-\tilde{S}_2^x, -\tilde{S}_2^y, \tilde{S}_2^z)$, $\mathbf{S}_3 = (-\tilde{S}_3^x, \tilde{S}_3^y, -\tilde{S}_3^z)$, and $\mathbf{S}_4 = (\tilde{S}_4^x, -\tilde{S}_4^y, -\tilde{S}_4^z)$. See (b) for an illustration of \mathbf{S} corresponding to $\tilde{\mathbf{S}} \parallel (1, 1, 1)$. (c) Spins illustrate two states in the “frustration-protected” compass manifold around the AFM Kitaev point $\psi = \pi/2$: Horizontal AFM chains arise through coupling $\propto J_K$. For any coupling $|J_H| \ll J_K$ along xx and zz bonds, contributions from up and down spins cancel and either orientation of the chain has the same energy [16]. Darker shading designates the dual lattice of every third upward pointing triangle, the vorticity in Fig. 3(e) was obtained for Wilson loops like the rhombus [17].

Here, however, the vortices are not induced by temperature T but persist for $T \rightarrow 0$. Their density is determined by the anisotropic couplings and they form a regular lattice maximizing their distance. We thus conclude that creating a vortex lowers the energy and that the vortices repel each other. The spin-structure factor is strongly peaked at three IC momenta, but has additional signals. The state may be related to an enigmatic phase of a strongly correlated quantum-spin-Hall (QSH) model [25].

We study the Hamiltonian

$$H = J_H \sum_{\langle i, j \rangle} \mathbf{S}_i \cdot \mathbf{S}_j + J_K \sum_{\gamma, \langle i, j \rangle \parallel \gamma} S_i^\gamma S_j^\gamma \quad (1)$$

where J_H is an isotropic Heisenberg coupling between classical spins \mathbf{S}_i on nearest neighbor (NN) sites $\langle i, j \rangle$ on the triangular lattice. The terms $\propto J_K$ are Ising-like and couple a different spin component S^γ (S^x , S^y , and S^z) on bonds along the three lattice directions γ , see Fig. 1(a).

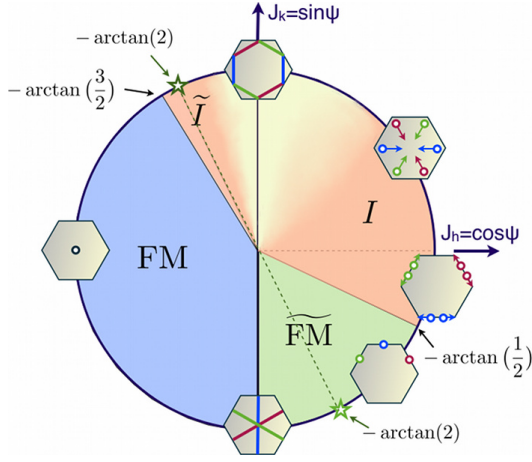


FIG. 2. (color online) Classical phase diagram of Eq. (1). The inset hexagons denote the first Brillouin zone, with colored markers (resp. line segments at $\psi = \pm\pi/2$) indicating the minima of the Fourier-transformed interactions $\mathcal{J}_\gamma(\mathbf{Q})$ [31]. Arrows indicate how they move when going around the circle in a counter-clockwise direction. The lighter shading around $\psi = \pi/2$, within the incommensurate regime, indicates a phase where Monte Carlo simulations show nematic correlations over wide temperature ranges. The right and left sides can be mapped onto each other by the four-sublattice transformation [13], mapping $\text{FM} \leftrightarrow \widetilde{\text{FM}}$ and $I \leftrightarrow \widetilde{I}$. The Kitaev points $\psi = \pm\pi/2$ map to themselves. Stars designate the hidden $\text{SO}(3)$ points $\widetilde{\text{AFM}}$ and $\widetilde{\text{FM}}$ at $\tan \psi = -2$. The AFM and $\widetilde{\text{AFM}}$ points are surrounded by incommensurate phases I and \widetilde{I} .

With $J_K = -2J_H > 0$, Eq. (1) was proposed for cobaltates [13] and also arises in a strong-coupling limit [26, 27] of a QSH model [25, 28], see the discussion toward the end of this Letter. For iridium ions in octahedral coordination and the bond geometry of the triangular lattice, ferromagnetic (FM) $J_H < 0$ and antiferromagnetic (AFM) $J_K > 0$ have been argued to arise from virtual hopping to e_g orbitals [29], while other processes lead to $J_H > 0$ and $J_K < 0$ [10]. As either sign can thus be argued to be relevant for either coupling, we investigate all relative strengths by parametrizing $J_H = \cos \psi$ and $J_K = \sin \psi$, with $\psi \in [0, 2\pi)$. In real space, Eq. (1) has translational invariance plus a two-fold axis perpendicular to the lattice. In spin space, $\text{SO}(3)$ symmetry is explicitly broken by the Kitaev terms and only mirror planes remain. Combining real and spin space gives the $D_{3d}(\bar{3}m)$ point group, the high- T space group of many layered triangular compounds of ABO_2 type.

First information about the classical phase diagram can be obtained by minimizing the Fourier transforms $\mathcal{J}_\gamma(\mathbf{Q})$ of the interaction [30, 31]. As can be seen in Fig. 2, the minima for the three spin components γ can be located at different IC momenta. Before going to the IC regime, which hosts the \mathbb{Z}_2 -vortex phase, we discuss special points and commensurate phases.

(Hidden) FM and AFM $\text{SO}(3)$ symmetric points.— The pure Heisenberg points for $\psi = 0, \pi$ ($J_K = 0$) have $\text{SO}(3)$ symmetry. The FM state at $\psi = \pi$ is moreover an eigenstate of the full quantum-mechanical model; the 120° pattern [32] at the AFM Heisenberg point $\psi = 0$ is not, but is expected to be stable against quantum fluctuations at $T = 0$ [33].

For $\tan \psi = -2$, the system has a “hidden” $\text{SO}(3)$ symmetry that becomes apparent after a four-sublattice spin rotation [13], see Fig. 1. The transformation preserves the form of the Hamiltonian (1), but changes $J_h \rightarrow J'_h = -J_h$ and $J_k \rightarrow J'_k = 2J_h + J_k$. The $\widetilde{\text{AFM}}$ point $\psi \simeq 0.6476\pi$ (where $J'_h > 0$ and $J'_k = 0$) was discussed in Ref. [13] and more recently in Refs. [26, 27]: The three sublattices of the 120° state together with the four sublattices of the transformation $\widetilde{\mathbf{S}} \leftrightarrow \mathbf{S}$ give a twelve-site unit cell with generally non-coplanar spins [34].

The $\widetilde{\text{FM}}$ counter point at $\psi \simeq -0.352\pi$ has unit cells containing up to four spins, with AFM spin patterns depending on the direction chosen by the rotated spin $\widetilde{\mathbf{S}}$. The FM and $\widetilde{\text{FM}}$ phases are quite stable against deviations from their respective (hidden) $\text{SO}(3)$ -symmetric point, see Fig. 2. As on the honeycomb lattice [15], quantum fluctuations favor a collinear AFM phase [27].

Kitaev points and nematic ordering at finite T .— For $\psi = \pi/2$ ($3\pi/2$) and $J_H = 0$, the lowest energy $E_0 = -|J_K|$ is reached by forming AFM (FM) Ising chains along one of the three lattice directions, with spins pointing along \hat{x} , \hat{y} , or \hat{z} [see 1(c)]. Flipping spins of a chain does not change the energy, leading to a degeneracy of 3×2^L states growing with the linear system size L . The sub-extensive degeneracy is related to a symmetry that is intermediate between local and global [35]. An accidental degeneracy actually allows further ground states with spins canted away from the axes [36], but Monte-Carlo (MC) simulations show this accidental degeneracy to be lifted by thermal fluctuations [31]. Such partial order into decoupled chains and a resulting nematic phase can also emerge in the low-energy limit of more complex models [37] and are in agreement with the analogous square-lattice ‘compass’ model, as is the entropic lifting of an accidental degeneracy [38, 39].

On the square lattice, two-dimensional long-range Néel order easily replaces the decoupled chains when the Hamiltonian deviates from the exact compass form [40, 41]. This remains true for our FM Kitaev point $J_K = -1$ ($\psi = 3\pi/2$): A small $J_H \neq 0$ couples the FM chains with an energy $\propto J_H L$ and stabilizes the FM ($\widetilde{\text{FM}}$) state for $J_H < 0$ ($J_H > 0$), leading to the sharp first-order transition between the FM and $\widetilde{\text{FM}}$ phases seen in Fig. 2.

Around the AFM Kitaev point $J_K \approx 1$ ($\psi \approx \pi/2$), on the other hand, each spin’s neighbors in an adjacent Ising-AFM chain compensate each other [16], see Fig. 1(c). MC simulations for $\psi = \text{atan } 4$, $\psi = \text{atan } 10$, and $\psi = \text{atan } 20$ support this, as they show partial order

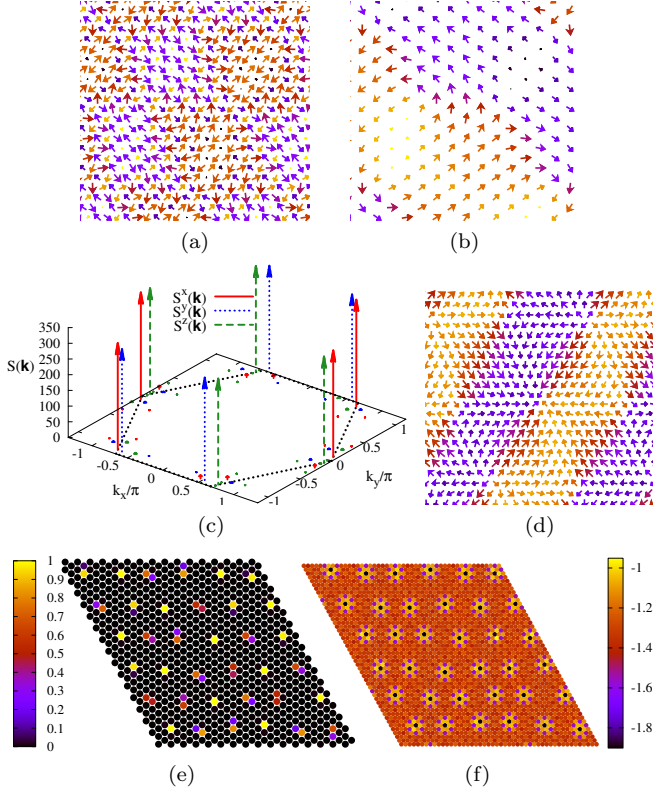


FIG. 3. (color online) (a) Spin pattern obtained by MC (down to $\beta = 96$) and subsequent optimization for $\tan \psi = -0.3$ and 48×48 sites. (b) Spin pattern on every third site and (c) spin-structure factors $S^\gamma(\mathbf{k})$ of (a). (d) shows the vector chirality $\kappa(\mathbf{r})$, Eq. (3), where vortices can be seen; (e) the corresponding vorticity of $\kappa(\mathbf{r})$ indicates strongly localized \mathbb{Z}_2 vortices [31]. (f) gives the local energy $e_{\mathbf{r}_i} = J_H \sum_{\delta} \mathbf{S}_{\mathbf{r}_i} \cdot \mathbf{S}_{\mathbf{r}_i+\delta} + J_K \sum_{\gamma, \delta \parallel \gamma} S_{\mathbf{r}_i}^\gamma \cdot S_{\mathbf{r}_i+\delta}^\gamma$, where δ denotes NN bonds. In (a), (b), and (d) shading refers to the out-of plane component from -1 (dark) to 1 (light yellow); for visibility, only part of the lattice is shown here, see [31] for full plots.

into decoupled chains over wide temperature ranges. At very low T , however, spins cant slightly away from the preferred direction and an IC non-coplanar ground state is selected.

\mathbb{Z}_2 -vortex phase.— The most intriguing phase is found around the AFM and $\bar{\text{AFM}}$ points. As they can be mapped onto each other [13], we focus here on the former, and in particular on $\psi \lesssim 0$ ($J_H > 0$, $J_K < 0$), which corresponds to the scenario of Ref. 10. For the 120° state at $\psi = 0$, the spin-structure factors

$$S^\gamma(\mathbf{k}) = \left| \sum_i e^{i\mathbf{k} \cdot \mathbf{r}_i} S_i^\gamma \right|^2 \quad (2)$$

are all peaked at the two K points, the corners of the first Brillouin zone. This state is also characterized by $|\kappa(\mathbf{r})| = 1$, where

$$\kappa(\mathbf{r}) = \frac{2}{3\sqrt{3}} (\mathbf{S}_{\mathbf{r}} \times \mathbf{S}_{\mathbf{r}+\mathbf{a}_1} + \mathbf{S}_{\mathbf{r}+\mathbf{a}_1} \times \mathbf{S}_{\mathbf{r}+\mathbf{a}_2} + \mathbf{S}_{\mathbf{r}+\mathbf{a}_2} \times \mathbf{S}_{\mathbf{r}}), \quad (3)$$

is the vector chirality on upward pointing triangles [shaded in Fig. 1(c)], with primitive lattice vectors $\mathbf{a}_{1,2}$.

When FM Kitaev-coupling J_K is switched on, spin patterns remain locally close to the 120° pattern, but are distorted at larger distances, see the spin configuration in Fig. 3(a) for $\tan \psi = -0.3$, which was obtained by MC down to $\beta = 96$ and subsequent spin optimization. The incommensurate modulation becomes clearer when looking at only one of the three sublattices of the 120° state, see Fig. 3(b). In momentum space, the dominant peaks of $S^\gamma(\mathbf{k})$ each move slightly away from K , see Fig. 3(c). Additional harmonics are small, but do not decrease for $T \rightarrow 0$. These additional features, which have been suggested to assist the formation of more complex states over spirals [42], allow the spin length to be 1 at every site and can be taken as a hint in favor of localized defects. Indeed, defects are clearly revealed in the site-dependent energy shown in Fig. 3(f) as well as in $|\kappa(\mathbf{r})|$ (not shown), which is reduced from 1 to ≈ 0.85 at the same locations.

Since we are close to the 120° state, whose order parameter has an $\text{SO}(3)$ space with the first homotopy group $\pi_1(\text{SO}(3)) = \mathbb{Z}_2$, localized topological defects are expected to be \mathbb{Z}_2 vortices [17]. Following Ref. 17, we thus calculate the rotation of $\kappa(\mathbf{r})$ when going around loops like the thick blue rhombus in Fig. 1(c) [31]. As Fig. 3(e) shows, the vorticity vanishes for most plaquettes, or adds to one on two neighboring plaquettes, indicating a rotation by 2π [43].

The formation of \mathbb{Z}_2 vortices is further elucidated by the form of the continuum limit. Following Ref. [44], a classical action for the long wavelength limit of Eq. (1) can be derived. We find that the Kitaev terms generate Lifshitz invariants, i.e. terms linear in gradients of the order parameter [45], in addition to exchange anisotropy terms. The gradient terms involve all three lattice directions and should dramatically alter the long-distance behaviour as compared to the pure AFM model ($J_K = 0$). The continuum limit implies that potential solutions are either (i) helicoidal one-dimensional modulations usually found in frustrated systems with Lifshitz invariants [45], or (ii) double-twisted states with localized cores as known from other highly symmetric systems, where Lifshitz invariants involve gradients in several spatial directions, as the blue phases of cholesteric liquid crystals [46] and chiral magnets [47]. Condensates of double-twisted states can create topological defects, which fits with the observation that the ground state of the lattice model (1) is given by \mathbb{Z}_2 vortices condensed into a defect-ordered phase, instead of a coplanar one-dimensional spiral state [48]. This suggests that the ‘double-twisting mechanism’ is operative around the \mathbb{Z}_2 vortices, and that the energy gain due to the twisting is more important than the loss at the vortex core, where the lattice cut-off possibly helps in bounding the latter.

Around the 120° state at $\psi = 0$, MC simulations consistently yield the \mathbb{Z}_2 phase down to the lowest T simu-

lated, both for $\psi < 0$ and $\psi > 0$. However, for some $0 < \psi \lesssim \pi/4$, we found vortex-free states with very slightly lower energy on smaller system sizes $L \leq 48$, e.g., -1.588 vs. -1.585 for $\psi = 0.15\pi = \arctan(0.5)$. Around the AFM Kitaev point $\psi = \pi/2$, the ground state remains IC and non-coplanar, but one spin component γ dominates. At low to intermediate T , a ‘frustration-protected’ manifold of (almost) decoupled AFM chains induces a nematic phase, see above and Fig. 1(c). Implementation and observation of ‘compass-model’-type physics, e.g. for the realization of protected qubits [8, 9, 41, 49, 50], might thus be more promising on such a frustrated than on a square lattice. It has not yet been clarified whether the transition between the two different IC phases is continuous or not, its approximate location is indicated by shading in Fig. 2.

Correlated QSH model.— As mentioned in the beginning, a situation similar to our model arises in the strongly correlated limit of a model for honeycomb iridates [25, 28]: Next-nearest neighbor sites, which form two triangular sublattices, are coupled by a combination of Ising and Heisenberg terms $\propto J_2$ that bring each sublattice close to the AFM point [26, 27]. AFM Heisenberg NN exchange J_1 couples the two sublattices and mediates an effective FM interaction within each, because the Néel AFM phase corresponds to FM order within a sublattice. When going from dominant J_1 to the AFM phase at large J_2 , the functional renormalization group has recently revealed IC magnetic order [26] for the quantum model. We have verified that the situation within the sublattices is indeed very close to our triangular lattice, in particular, the IC phase of the classical honeycomb model is likewise non-coplanar and \mathbb{Z}_2 -vortices can be identified.

Conclusions.— We have investigated an anisotropic spin-orbit model given by Kitaev-like couplings on a triangular lattice, which also describes some features of correlated spin-orbit-coupled electrons on a honeycomb lattice. In addition to nematic and commensurate phases, the classical limit of the model has IC and noncoplanar phases characterized by localized defects, topologically stable \mathbb{Z}_2 vortices. In contrast to well-known entropy-driven \mathbb{Z}_2 vortices [17, 23], the defects are here stabilized by the ‘Kitaev’-type anisotropic spin-orbit couplings and persist for $T \rightarrow 0$. We have thus found a \mathbb{Z}_2 analog to the \mathbb{Z} -vortex phases of type-II superconductors [52] and liquid crystals (the twist-grain-boundary state [53]), and to the Skyrmion lattices in chiral magnets [54].

Such localized-defect states could be realized in triangular quasi-two-dimensional lattices of $5d$ ions (e.g. iridium) with strong spin-orbit interaction and electronic correlations. It is noteworthy that the zigzag pattern of Na_2IrO_3 [51] is the AFM phase of the Kitaev-Heisenberg model on the honeycomb lattice [29], the coupling regime of potential triangular-lattice compounds

can consequently be expected to be close to the AFM point as well, i.e., within the regime of the \mathbb{Z}_2 -vortex lattice. Optical lattices modelling spin-orbit coupled systems might similarly provide a route [55]. While we have concentrated on a spin(-orbit) model, itinerant carriers raise further possibilities, because a non-coplanar spin-background can induce topologically non-trivial bands [56, 57]. It is thus intriguing to consider relations between the \mathbb{Z}_2 -vortex phase on the honeycomb model to an enigmatic QSH* state of the corresponding Hubbard model [25].

This research was sponsored by the Deutsche Forschungsgemeinschaft (DFG) under the Emmy-Noether program. We thank G. Khaliullin for helpful discussion.

-
- [1] K. I. Kugel and D. I. Khomskii, *Soviet Physics Uspekhi* **25**, 231 (1982).
 - [2] A. Kitaev, *Ann. Phys.* **321**, 2 (2006).
 - [3] G. Chen, L. Balents, and A. P. Schnyder, *Phys. Rev. Lett.* **102**, 096406 (2009).
 - [4] G. Khaliullin and S. Maekawa, *Phys. Rev. Lett.* **85**, 3950 (2000).
 - [5] J. Chaloupka and A. M. Oleś, *Phys. Rev. B* **83**, 094406 (2011).
 - [6] D. Pesin and L. Balents, *Nat. Phys.* **6**, 376 (2010).
 - [7] J. W. Venderbos, M. Daghofer, and J. van den Brink, *Phys. Rev. Lett.* **107**, 116401 (2011); J. W. F. Venderbos, S. Kourtis, J. van den Brink, and M. Daghofer, *Phys. Rev. Lett.* **108**, 126405 (2012).
 - [8] B. Douçot, M. Feigel’man, L. Ioffe, and A. Ioselevich, *Phys. Rev. B* **71**, 024505 (2005).
 - [9] Z. Nussinov and E. Fradkin, *Phys. Rev. B* **71**, 195120 (2005).
 - [10] G. Jackeli and G. Khaliullin, *Phys. Rev. Lett.* **102**, 017205 (2009).
 - [11] G. Chen and L. Balents, *Phys. Rev. B* **78**, 094403 (2008).
 - [12] B. J. Kim, H. Ohsumi, T. Komesu, S. Sakai, T. Morita, H. Takagi, and T. Arima, *Science* **323**, 1329 (2009).
 - [13] G. Khaliullin, *Prog. Theor. Phys. Suppl.* **160**, 155 (2005).
 - [14] J. Kim, A. H. Said, D. Casa, M. H. Upton, T. Gog, M. Daghofer, G. Jackeli, J. van den Brink, G. Khaliullin, and B. J. Kim, *arXiv:1205.5337*.
 - [15] J. Chaloupka, G. Jackeli, and G. Khaliullin, *Phys. Rev. Lett.* **105**, 027204 (2010).
 - [16] T. Eggarter, *Phys. Rev. B* **12**, 1933 (1975).
 - [17] H. Kawamura and S. Miyashita, *J. Phys. Soc. Jpn.* **53**, 4138 (1984).
 - [18] J.-C. Dornenge, C. Lhuillier, L. Messio, L. Pierre, and P. Viot, *Phys. Rev. B* **77**, 172413 (2008).
 - [19] H. Kawamura, A. Yamamoto, and T. Okubo, *J. Phys. Soc. Jpn.* **79**, 023701 (2010).
 - [20] H. Kawamura, *J. Phys.: Conf. Ser.* **320**, 012002 (2011).
 - [21] R. Tamura, S. Tanaka, and N. Kawashima, *arXiv:1209.2520*.
 - [22] G. Toulouse and M. Kléman, *J. Physique Lett.* **37**, 149 (1976).
 - [23] P. W. Anderson and G. Toulouse, *Phys. Rev. Lett.* **38**,

- 508 (1977).
- [24] J. Lovegrove, M. O. Borgh, and J. Ruostekoski, *Phys. Rev. A* **86**, 013613 (2012).
 - [25] A. Rüegg and G. A. Fiete, *Phys. Rev. Lett.* **108**, 046401 (2012).
 - [26] J. Reuther, R. Thomale, and S. Rachel, [arXiv:1206.3103](#).
 - [27] M. Kargarian, A. Langari, and G. A. Fiete, [arXiv:1207.2156](#).
 - [28] A. Shitade, H. Katsura, J. Kuneš, X.-L. Qi, S.-C. Zhang, and N. Nagaosa, *Phys. Rev. Lett.* **102**, 256403 (2009).
 - [29] J. Chaloupka, G. Jackeli, and G. Khaliullin, [arXiv:1209.5100](#).
 - [30] J. M. Luttinger and L. Tisza, *Phys. Rev.* **70**, 954 (1946).
 - [31] See supplemental material at...
 - [32] Y. Yafet and C. Kittel, *Phys. Rev.* **87**, 290 (1952).
 - [33] N. Elstner, R. R. P. Singh, and A. P. Young, *Phys. Rev. Lett.* **71**, 1629 (1993).
 - [34] Spins \mathbf{S} are only coplanar if the plane formed by the \tilde{S} is orthogonal to a NN bond.
 - [35] Z. Nussinov and G. Ortiz, *PNAS* **106**, 16944 (2009); Z. Nussinov, C. D. Batista, and E. Fradkin, *Int. J. Mod. Phys.* **20**, 5239 (2006).
 - [36] In contrast to the compass model, this includes here non-coplanar patterns.
 - [37] S. Liang, M. Daghofer, S. Dong, C. Sen, and E. Dagotto, *Phys. Rev. B* **84**, 024408 (2011); J. W. F. Venderbos, M. Daghofer, J. van den Brink, and S. Kumar, *Phys. Rev. Lett.* **107**, 076405 (2011).
 - [38] A. Mishra, M. Ma, F.-C. Zhang, S. Guertler, L.-H. Tang, and S. Wan, *Phys. Rev. Lett.* **93**, 207201 (2004).
 - [39] S. Wenzel and W. Janke, *Phys. Rev. B* **78**, 064402 (2008).
 - [40] L. Cincio, J. Dziarmaga, and A. M. Oleś, *Phys. Rev. B* **82**, 104416 (2010).
 - [41] F. Trouselet, A. M. Oleś, and P. Horsch, *EPL* **91**, 40005 (2010).
 - [42] H. Shiba and N. Suzuki, *J. Phys. Soc. Jpn.* **52**, 1382 (1983).
 - [43] If all rotations along a loop were around the same axis, the vorticity would be quantized to 0 or 1 on each individual plaquette. As the rotation axes can vary, this does not have to hold.
 - [44] T. Dombre and N. Read, *Phys. Rev. B* **39**, 6797 (1989); P. Azaria, B. Delamotte, F. Delduc, and T. Jolicoeur, *Nucl. Phys. B* **408**, 485 (1993).
 - [45] I. Dzyaloshinskii, *Sov. Phys. JETP* **19**, 960 (1964).
 - [46] D. C. Wright and N. D. Mermin, *Rev. Mod. Phys.* **61**, 385 (1989).
 - [47] A. N. Bogdanov and D. A. Yablonskii, *Sov. Phys. JETP* **68**, 101 (1989).
 - [48] A simple superposition of helices would moreover not allow a spin length of 1 at every site.
 - [49] F. Trouselet, A. Oleś, and P. Horsch, [arXiv:1207.0102](#).
 - [50] S. Gladchenko, D. Olaya, E. Dupont-Ferrier, B. Douçot, L. B. Ioffe, and M. E. Gershenson, *Nat. Phys.* **5**, 48 (2008).
 - [51] X. Liu, T. Berlijn, W.-G. Yin, W. Ku, A. Tsvelik, Y.-J. Kim, H. Gretarsson, Y. Singh, P. Gegenwart, and J. P. Hill, *Phys. Rev. B* **83**, 220403 (2011).
 - [52] A. A. Abrikosov, *Sov. Phys. JETP* **5**, 1174 (1957).
 - [53] S. R. Renn and T. C. Lubensky, *Phys. Rev. A* **38**, 2132 (1988).
 - [54] A. N. Bogdanov and A. Hubert, *J. Magn. Magn. Mater.* **138**, 255 (1994); U. K. Röbber, A. N. Bogdanov, and C. Pfleiderer, *Nature* **442**, 797 (2006).
 - [55] Y. J. Lin, K. Jiménez-García, and I. B. Spielman, *Nature* **471**, 83 (2011).
 - [56] P. Matl, N. Ong, Y. Yan, Y. Li, D. Studebaker, T. Baum, and G. Doubinina, *Phys. Rev. B* **57**, 10248 (1998).
 - [57] Y. Taguchi, Y. Oohara, H. Yoshizawa, N. Nagaosa, and Y. Tokura, *Science* **291**, 2573 (2001).

Supplemental material

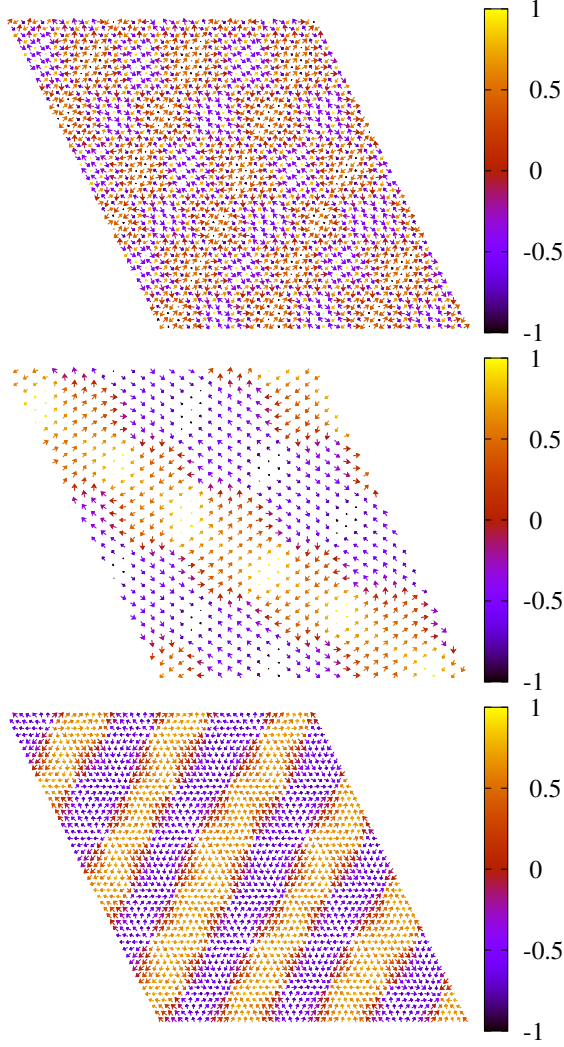


FIG. 4. (color online) Full-lattice versions for Figs. 3(a), (b), and (d) of the main text.

In this supplemental material, we provide some technical notes and additional data supporting the conclusions presented in the main text. As our most prominent point is the discovery of a \mathbb{Z}_2 -vortex lattice, the first Section gives details on how the \mathbb{Z}_2 vortices were identified from the Markov-chain Monte-Carlo (MCMC) data. The second part discusses issues related to the other phases and the phase diagram, Fig. 2 of the main text.

Identification of \mathbb{Z}_2 vortices

Figure 4 shows the whole 48×48 site lattice for the figures shown in Figs. 3(a), (b), and (d) of the main text, where only part of the lattice is displayed for visibility. The vorticity of $\kappa(\mathbf{r})$ was calculated by going

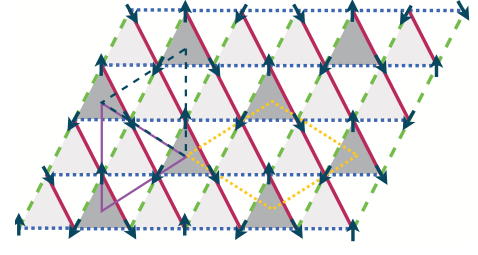


FIG. 5. (Color online) Upward pointing triangles (shaded) of the triangular lattice, for which $\kappa(\mathbf{r})$ is calculated. Dark shading denotes every third upward-pointing triangle, the vorticity of $\kappa(\mathbf{r})$ is evaluated on loops connecting these darker triangles. The smallest possible loops are right- and left-pointing triangles, information from both has to be combined to cover the original lattice. When using rhombus loops connecting four dark triangles, one rhombus-lattice covers the whole lattice. These latter loops were used to obtain the figures shown here and in the main text. Arrows illustrate the 120° pattern, the vector chirality $\kappa(\mathbf{r})$ on shaded triangles points out of the plane.

around loops as shown in Fig. 1(c) of the main text, i.e., from $\kappa(\mathbf{r})$ on every third of the upward-pointing triangles. This dual lattice in turn forms again a triangular lattice, the geometry of the original and dual lattices can be seen in Fig. 5.

We closely follow Ref. 1, with one exception: our vorticity is rescaled to be 0 for no rotation and 1 for a rotation by 2π , as opposed to 1 and -1 , resp. In order to determine the rotation between two plaquettes of the dual lattice connected by an edge of the loop, we need two vectors on each plaquette, as a single vector $\kappa(\mathbf{r})$ would not determine the rotation axis. We tried three approaches: (i) using one spin on each plaquette as the second vector, [1] (ii) using $\kappa(\mathbf{r})$ of the adjacent downward pointing triangle, and (iii) not using a second vector and instead choosing the rotation axis as orthogonal to the plane spanned by the two $\kappa(\mathbf{r})$ -vectors. All three approaches lead to equivalent results near the 120° order, and all three suffer from difficulties once the vortices become very dense and a local 120° pattern can no longer be robustly assigned. Figures presented were obtained with approach (iii).

We additionally calculated the vorticity for smaller loops connecting only three plaquettes that form right- and left-pointing triangles, see Fig. 5. The results are equivalent. We also verified that the results remain unchanged, when the dual lattice is constructed from the downward pointing triangles of the original lattice.

Fourier transform of the Kitaev-Heisenberg interactions

Since we are dealing with a Bravais lattice and classical spins, a promising start is the so-called Luttinger-Tisza

method.[2] With $\mathbf{S}_{\mathbf{k}} \equiv \sum_{\mathbf{r}} e^{i\mathbf{k}\cdot\mathbf{r}} \mathbf{S}_{\mathbf{r}}$, the classical energy per site reads

$$\epsilon_{\text{cl}} = \sum_{\mathbf{k}, \gamma} \mathcal{J}_{\gamma}(\mathbf{k}) S_{\mathbf{k}}^{\gamma} S_{-\mathbf{k}}^{\gamma}, \quad \text{where} \quad (4)$$

$$\begin{aligned} \mathcal{J}_x(\mathbf{k}) &= J_h [\cos(\mathbf{k} \cdot \mathbf{l}_y) + \cos(\mathbf{k} \cdot \mathbf{l}_z)] + (J_h + J_k) \cos(\mathbf{k} \cdot \mathbf{l}_x), \\ \mathcal{J}_y(\mathbf{k}) &= \mathcal{J}_x(\mathbf{R}_{\frac{2\pi}{3}} \cdot \mathbf{k}), \quad \mathcal{J}_z(\mathbf{k}) = \mathcal{J}_x(\mathbf{R}_{-\frac{2\pi}{3}} \cdot \mathbf{k}). \end{aligned} \quad (5)$$

Here $\mathbf{l}_y = \mathbf{x}$, $\mathbf{l}_z = (\mathbf{x} + \sqrt{3}\mathbf{y})/2$, $\mathbf{l}_x = \mathbf{l}_z - \mathbf{l}_y$ are primitive vectors of the lattice, and $\mathbf{R}_{\pm \frac{2\pi}{3}}$ stand for C_3 rotations around the z -axis in momentum space. For a large regime of $-\text{atan}(3/2) < \psi < 3\pi/2$, all three $\mathcal{J}_{\gamma}(\mathbf{k})$ are minimized at $\mathbf{k} = (0, 0)$, indicating a FM state. Here the ground state (GS) energy does not change by global rotations of the spins, and so the GS manifold has a continuous accidental degeneracy (except for $\psi = \pi$ where the degeneracy is related to the global $\text{SO}(3)$ symmetry).

For the range $3\pi/2 < \psi < -\text{atan}(1/2)$ the three minima are at the M points of the first Brillouin zone, i.e., the midpoint of the sides of the hexagon, with each \mathcal{J}_{γ} being minimum at a different side. This is the signature of the commensurate order that can be seen as the $\widetilde{\text{FM}}$ phase. Since the three M points are one-half of a reciprocal vector, one can generate a continuous family of ground states by forming linear combinations of the three modulations without violating the unit length constraint.[3] The resulting GS manifold has a two-dimensional structure continuously connecting the three M points. In the rotated frame (defined by the transformation $\mathbf{S} \rightarrow \widetilde{\mathbf{S}}$, see main text), this is nothing but the accidental degeneracy related to global rotations (again, except for the $\widetilde{\text{FM}}$ point where the degeneracy is symmetry related).

Directly at the pure Kitaev points $\psi = \pi/2, 3\pi/2$, each $\mathcal{J}_{\gamma}(\mathbf{k})$ is minimal along a *line* in momentum space, a signature of the decoupled chains and the “intermediate symmetry” (see main text), as in the square-lattice compass model. The GS manifold has an additional continuous accidental degeneracy which will be discussed elsewhere.

In the remaining range $-\text{atan}(1/2) < \psi < -\text{atan}(3/2)$, each $\mathcal{J}_{\gamma}(\mathbf{k})$ is peaked at a different incommensurate [4] momentum $\mathbf{k} = \mathbf{Q}_{\gamma}$ for each spin component γ , which are related by C_3 rotations. Consequently, not all three spin components can be minimized simultaneously with a single \mathbf{Q}_{γ} . If one were able to do so, or even if one were able to optimize only two components γ at the same

$\mathbf{k} = \mathbf{Q}$, the problem could be solved by a coplanar spiral $\mathbf{S}_{\mathbf{r}}/S = \cos(\mathbf{Q} \cdot \mathbf{r})\mathbf{e}_1 + \sin(\mathbf{Q} \cdot \mathbf{r})\mathbf{e}_2$, where the two vectors \mathbf{e}_1 and \mathbf{e}_2 define the spin plane. As there is however *no* momentum that minimizes simultaneously the energy for more than one spin component, there is no way to form a ground state through a coplanar incommensurate spiral.

Compass-like phases at the Kitaev point

Figure 6 shows that - as in the square-lattice compass model - low- T states have spins polarized along one of the three axes, even though the ground-state manifold has an additional accidental degeneracy and contains also non-collinear and even non-coplanar states.

-
- [1] H. Kawamura and S. Miyashita, *J. Phys. Soc. Jpn.* **53**, 4138 (1984).
 - [2] J. M. Luttinger and L. Tisza, *Phys. Rev.* **70**, 954 (1946).
 - [3] J. B. Fouet, P. Sindzingre, and C. Lhuillier, *Eur. Phys. J. B* **20**, 241 (2001).
 - [4] With the exception of the AFM and $\widetilde{\text{AFM}}$ points, which lie within this range, where the peaks are at K (the corner of the BZ) and halfway between Γ and K , [13] respectively.
 - [5] G. Khaliullin, *Progr. Theor. Phys. Suppl.* **160**, 155 (2005).

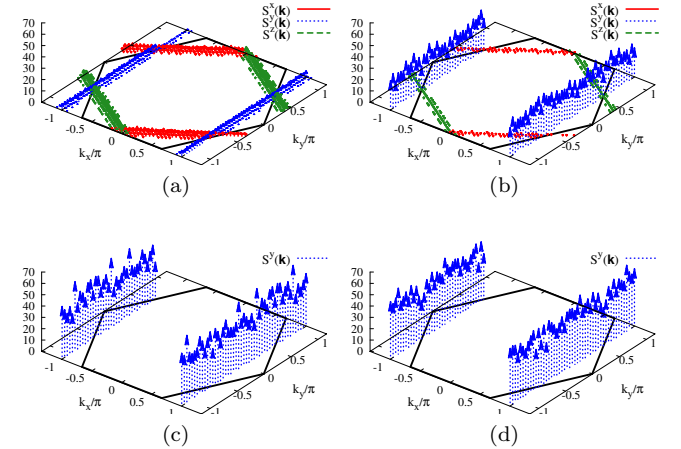


FIG. 6. (color online) Spin-structure factors $S^{\gamma}(\mathbf{k})$ for $\psi = \pi/2$ and inverse temperature (a) $\beta = 1/k_B T = 8$, where signals in all three components are visible, (b) $\beta = 10$, (c) $\beta = 100$, and (d) $\beta = 1000$, where decoupled chains along one direction dominate.